

ULRR

Initial evaluation of the performance of novel inorganic scintillating detectors for small animal irradiation dosimetry

Item Type	Article
Authors	Byrne, Kevin;Alharb, Majed;Esplen, Nolan;Woulfe, Peter;O'Keeffe, Sinéad;Bazalova-Carter, Magdalena;Foley, Mark
Citation	IEEE Sensors Journal; 20 (9)
Publisher	IEEE Computer Society
Download date	2026-03-16 21:06:47
Item License	https://creativecommons.org/licenses/by-nc-sa/1.0/
Link to Item	https://hdl.handle.net/10344/8646

Initial evaluation of the performance of novel inorganic scintillating detectors for small animal irradiation dosimetry

K. Byrne, M. Alharbi, N. Esplen, P. Woulfe, S. O’Keeffe, M. Bazalova-Carter, M. Foley.

Abstract — The purpose of this study was to design and evaluate the performance of four novel inorganic scintillating detectors (ISDs) on the Small Animal Radiation Research Platform (SARRP). Relative scintillator output, measurement repeatability, setup uncertainty, linearity with dose rate, and signal reproducibility over time were investigated. The Gd₂O₂S:Tb detector had the highest relative signal output, generating up to 219 times more charge than a previously characterized BCF-60-based plastic scintillating detector (PSD). The Gd₂O₂S:Tb detector was then used to measure 220 kVp therapy beam profiles of 10 x 10 and 5 x 5 mm² fields. Beam profiles using the ZnS-based phosphor were also obtained and compared to investigate the performance of a lower density inorganic scintillator. 10 x 10 and 5 x 5 mm² therapy beam profile measurements made with the Gd₂O₂S:Tb and BCF-60 detectors differed, on average, by 1.1% and 1.9%, respectively. The ZnS:Ag measurements differed, on average, by 2.5% and 6% relative to BCF-60 measurements of the 10 x 10 and 5 x 5 mm² beam profiles, respectively. MicroCT imaging of the detector volumes was also performed, revealing poor packing of the ZnS:Ag crystalline phosphor in the deepest region of the cylindrical cavity. The Gd₂O₂S:Tb detector, in particular, has proven to be a promising candidate for real-time dosimetry of small fields in small animal irradiators, primarily because of the very large signal intensities observed, along with good repeatability, dose rate linearity, reproducibility and agreement with beam profile measurements made with a previously validated detector.

Index Terms — dosimetry, optical fibers, radiation detectors, scintillators.

I. INTRODUCTION

EXPERIMENTS in preclinical trials are essential to both the study of radiobiology and the advancement of clinical radiation oncology. Animal models have been used for decades to provide scientists and clinicians an insight into disease processes and to assist in the development of new strategies to prevent, cure and mitigate cancer and radiation effects. Mouse models are often utilized because of their cost

effectiveness and versatility when studying tumor and normal tissue radiobiology and, therefore, preclinical trials involving mice are now a standard component of oncology research. The use of animal models not only reduces the exposure of humans to harmful substances and treatments, but has also proven vital to our understanding of the molecular and physiological mechanisms of radiation response [1].

Imaging and irradiation technologies have significantly advanced in preclinical contexts to allow for highly conformal image-guided irradiations of small animals in an effort to mimic human treatment capabilities, albeit with some biological and physical limitations [1]. To support the delivery of increasingly sophisticated radiotherapy techniques, small animal irradiators have been designed to reproduce these techniques for preclinical studies and better facilitate translational research [2], [3]. These irradiators generally operate at kilovoltage energies and employ small field sizes ($\leq 1 \times 1 \text{ cm}^2$), making high spatial-resolution dosimetry vital in ensuring high accuracy and precision for treatment verification and quality assurance [4]. On-board imaging systems provide improved targeting and precise positioning, but also require adapted quality control, beam dosimetric characterization and treatment monitoring [5]. This advanced pre-clinical technology requires accurate and precise real-time dosimeters [6].

However, these needs are not sufficiently met by the common dosimetry technologies of today. Ionization chambers, for example, are well adapted for reference beam dosimetry in large fields, but their large active volumes create spatial resolution problems when used in small beams [4]. Films offer high spatial resolution but cannot provide dose measurement in real time. Thermoluminescent dosimeters (TLDs) suffer from both the inability to provide direct read-outs and from deficiencies with regards to spatial resolution. Although silicon diodes (SiD) and metal-oxide semiconductor field-effect transistors (MOSFETs) can both provide measurements in real-time and provide high spatial resolution capabilities, they both suffer from energy and orientation-based dependencies. SiDs

Manuscript submitted November 19, 2019. This work was supported in part by the Irish Association of Physicists in Medicine through the 2019 Young Investigator Grant.

Kevin Byrne is an M.Sc. graduate and Walton scholarship recipient in Medical Physics at the National University of Ireland, Galway. (email: kevin.byrne56@mail.dcu.ie)

Majed Alharbi is a PhD student of Medical Physics at the National University of Ireland, Galway. (e-mail: m.alharbi2@nuigalway.ie)

Nolan Esplen is a PhD student of Medical Physics at the University of Victoria, British Columbia, Canada. (e-mail: nolane@uvic.ca)

Peter Woulfe is a chief medical physicist at the Galway Clinic, Galway.

(e-mail: peter.woulfe@galwayclinic.ie)

Dr. Sinead O’Keeffe is a research fellow at the University of Limerick. (e-mail: sinead.okeeffe@ul.ie).

Dr. Magdalena Bazalova-Carter is an Assistant Professor and Canada Research Chair in Medical Physics (Tier 2) at the University of Victoria, British Columbia, Canada. (e-mail: bazalova@uvic.ca)

Dr. Mark Foley is the Academic Director of the CAMPEP accredited MSc in Medical Physics at the National University of Ireland, Galway. (e-mail: mark.foley@nuigalway.ie)

also cause a high level of dose perturbation in radiation beams and MOSFET-based detectors suffer a brief radiation-lifetime of around 200 Gy. Electronic Portal Imaging Devices (EPIDs), while otherwise desirable, exhibit persistent signal after irradiation cessation, known as “ghosting”, and are extremely sensitive to lower energy photons of their own construction [7].

Optical fiber dosimeters (OFDs), by contrast with the aforementioned detectors, provide real-time measurements and can be designed with small sensitive volumes, making them a promising technology for use in small-field dosimetry applications [6]. The drawbacks of OFDs surround unwanted optical signal generation within the signal-carrying optical fiber (OF), known as stem effects [8]. Stem effects consist mostly of Cerenkov radiation [9] which, in the case of polymethyl methacrylate (PMMA), is a phenomena that occurs at energies higher than approximately 178 keV [10], and optical fiber fluorescence. OFDs are typically created using plastic (organic) scintillating detectors (PSDs) due to their water-equivalence, energy independence and short response time, but suffer from low light output (especially at low energies). Inorganic scintillator materials, although known to suffer from energy-dependencies and poor tissue-matching qualities, have superior light output, making them an attractive option for the dosimetry of small fields at kV energies. Inorganic scintillators also have superior radiation hardness compared to plastic scintillating materials and their compositions span over a wide range of atomic numbers, thus scintillating over a wide range of wavelengths, which makes them compatible with a wider range of apparatus [11].

OFDs using inorganic scintillating detectors (ISDs) have recently begun to be utilized across a range of medical imaging and radiotherapy dosimetry applications [12]–[14]. Our work investigates novel ISD designs fabricated using a phosphor-filled micromachined cavity in the PMMA optical fiber core. Four different inorganic scintillating phosphors were evaluated to explore further the potential applications of ISDs in small animal radiation dosimetry.

As the dosimeter design incorporates a PMMA optical fiber, it was necessary to consider the stem effect contributions to the fiber output signal. Many attempts have been made to quantify or discriminate such signals in optical fiber dosimeters for both kV and MV beam energies [8], [15]–[17]. Le Deroff *et al.*[17] irradiated 194 cm of PMMA optical fiber lacking an active scintillating volume with beam energies set at 225, 100 and 40 kVp while applying maximum tube currents to maximize the stem effect signal (13, 30 and 45 mA for 225, 100 and 40 kVp, respectively). The negligible signal generated in this experiment was indicative of the inability of beam energies ≤ 225 kV to produce secondary electrons capable of causing detectable Cerenkov effects within the optical fiber. The stem effect is, therefore, exclusively composed of optical fiber fluorescence and typically contributes to less 0.1% of the signal, which requires no correction [6].

In this study, we present the initial evaluation of four novel scintillating detector designs using various inorganic scintillating phosphors for the 40 and 80 kVp imaging beams and 220 kVp therapy beam of the Small Animal Radiation Research Platform (SARRP) [2].

II. DETECTOR DESIGN

A representative design (which was adapted from a previous design by Alharbi *et al.* [18]) schematic for the OFDs is illustrated in Figure 1. Each ISD consisted of a 1 mm diameter, 1 m long cladded PMMA optical fiber made light-tight by a 0.6 mm thick protective polyethylene jacket, and a SubMiniature version A (SMA) connection at one end. The sensing end was micro-machined to make a 700 μm diameter, 3 mm long cavity. The design diameter was influenced by the need for increased spatial resolution, whereas the length dimension was chosen as a precaution considering the possible difficulties that might be encountered when filling a 700 μm diameter cavity with the crystal phosphors. In anticipation of possible ‘dead-space’ in the PMMA cavity reducing the overall signal output of the ISDs, a 3 mm length was chosen to increase the haptic sensation of successful cavity-filling and to guarantee that a comparable amount of phosphor would be present within each detector cavity. Each cavity was packed with a different inorganic scintillating phosphor powder ($\text{Gd}_2\text{O}_2\text{S:Tb}$, $\text{Gd}_2\text{O}_2\text{S:Eu}$, $\text{Gd}_2\text{O}_2\text{S:Pr}$, ZnS:Ag)(Phosphor Technology Ltd., Stevenage, UK) and sealed with an opaque epoxy. Black insulating tape was also used to provide additional optical shielding around the active volume. The SMA connection was used to attach each detector to a further 20 m optical fiber cable.

To provide a comparison for the performance of the ISDs in terms of light output and beam profile measurements, a PSD which consisted of a polystyrene scintillating fiber (BCF-60, Saint-Gobain Crystals, Nemours, France) with a 1 mm diameter, 1 mm long active volume [6] was included in the study. The active volume was protected by a 0.015 mm thick PMMA cladding. This was optically coupled to a 1 mm diameter, 15 m long cladded PMMA optical fiber, also made light-tight by a 0.6 mm thick black polyethylene jacket.

The 20 m OF extension the and 15 m OF used for the inorganic and plastic scintillating detectors, respectively, were terminated by connection through an adapter to an H10721 photomultiplier tube (Hamamatsu Photonics, Hamamatsu, Japan). The photomultiplier tube was connected to a UNIDOS E electrometer (PTW, Freiburg, Germany) outputting nC-sensitive charge readings in real time. The measured charge was used as a surrogate for the light generated within the scintillator. Key characteristics for each scintillator used are summarized in Tables 1a and 1b.

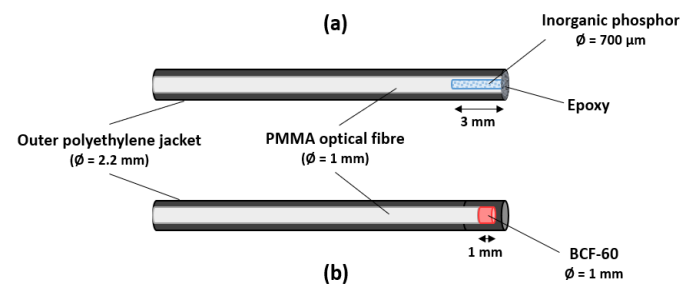


Fig. 1. Schematic representation of the optical fiber detector designs, where (a) depicts the ISD design (adapted from M. Alharbi *et al.* [18]) with the phosphor packed cavity shown in blue, and (b) depicts the PSD design with the optically coupled BCF-60 active volume in red.

TABLE 1A

A SUMMARY OF THE CHARACTERISTICS OF EACH INORGANIC SCINTILLATOR USED [14], [19]–[21]

Inorganic Scintillator	Density (g/cm ³)	Z _{eff}	Median Particle Size (μm)	Emission Wavelength (nm)	Decay time (ns)	Photons/MV
Gd ₂ O ₂ S:Tb	7.3	~ 60	10.0	545 (green)	~ 3 × 10 ⁵	~ 60 000
Gd ₂ O ₂ S:Eu	7.3	~ 60	9.0	610 (red)	~ 5 × 10 ⁶	~ 60 000
Gd ₂ O ₂ S:Pr	7.3	~ 60	8.1	513 (green)	~ 5 × 10 ³	~ 50 000
ZnS:Ag	4.1	~ 27	10.7	460 (blue)	~ 5 × 10 ²	~ 90 000

TABLE 1B

A SUMMARY OF THE CHARACTERISTICS OF THE ORGANIC SCINTILLATOR USED [22]

Organic Scintillator	Density (g/cm ³)	Z _{eff}	Emission Wavelength (nm)	Decay time (ns)	Photons/MV
BCF-60	1.05	~ 5.7	530 (green)	~ 7	~ 7 100

III. IRRADIATIONS

All irradiations were carried out on the SARRP (Xstrahl Inc., Suwanee, GA, USA) located at the University of Victoria, BC, Canada. The SARRP 220 kVp (therapy), 40, and 80 kVp (imaging) beam energies were utilized with focal spot sizes of 3.0 and 0.4 mm (IEC366) for the therapy and imaging beams, respectively. The SARRP has 0.8mm Be internal filtration with an external filtration of 0.15mm Cu for the 220 kVp therapy beam and a 1 mm Al external filtration for the imaging beams [6]. The PMT was held at a potential difference of +700 mV and irradiations occurred at a source-to-detector distance (SDD) of 33 cm unless otherwise stated. A schematic of the setup is seen in Figure 2.

The arrangement of the detectors on the 5 mm thick polystyrene bed is shown in Figure 3, where the beam direction (z) is orthogonal to the plane (x, y) of the removable SARRP bench shown. The positions of the detector arrangement were fixed to the irradiation stage of the SARRP for the entire study. The positioning of the detectors within the irradiation fields were then controlled solely by the SARRP positioning software, which is known to have a positional uncertainty of just ±0.20 mm.

Dark current values (expressed in nC.s⁻¹) were determined for all measurement series of each sensor every time the apparatus was adjusted by calculating the average of three electrometer readings taken without exposing the connected detector. These dark current values were then multiplied by the total “electrometer on” time and subtracted from the total charge reading on the electrometer for each measurement. Due to the difficulty of the SARRP to ramp-up to 220 kVp and fall to 0.1 mA at the beginning of irradiations, electrometer measurements were initiated some time (dt₁) prior to “beam on” and terminated some time following “beam off” (dt₂). A brief series of measurements with varying pre- and post- beam-on times (dt₁ and dt₂) resulted in no measurable effect on the net charge measured. This concept is shown graphically in Figure 4. The depiction of signal in red represents the signal that would have been lost while waiting for the SARRP output to stabilize before beginning charge measurement 5 s after the initial beam ramp-up, as described by Johnstone *et al.*[6]

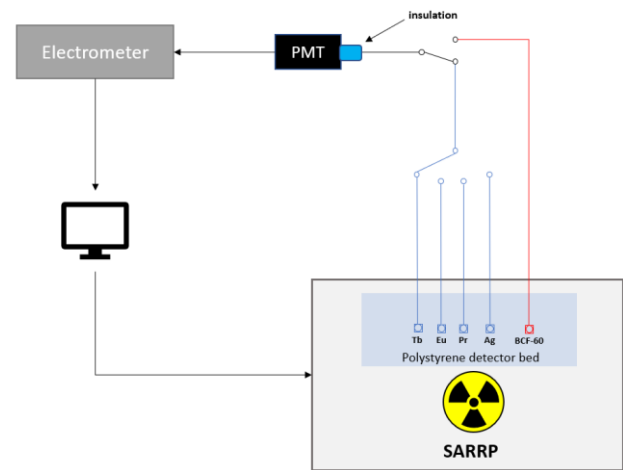


Fig. 2. Schematic representation of the experimental setup. The four blue connections depict the ISDs, whereas the red one depicts the PSD.

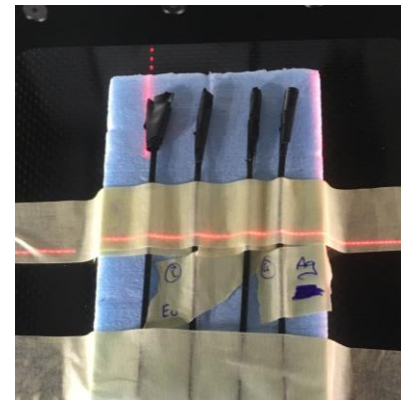


Fig. 3. Photograph taken during the laser alignment process for the inorganic scintillators on the polystyrene detector bed affixed to the removable treatment bench. From left to right: Gd₂O₂S:Tb, Gd₂O₂S:Eu, Gd₂O₂S:Pr and ZnS:Ag. The horizontal (x) and vertical (y) axes of the figure are orthogonal to the beam direction (z).

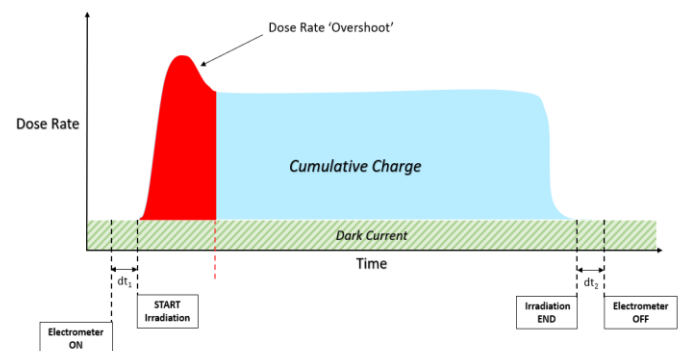


Fig. 4. Graphical representation of the signal of interest in blue and the dark current in green to be subtracted from the electrometer reading. The figure also shows an exemplar ‘overshoot’ of radiation dose which is possible during irradiation at 0.1 mAs.

A. Output Intensity, Repeatability and Linearity

A measure of the relative output intensity of each scintillator

signal was made. 60 s irradiations, centered in a 10 x 10 mm² square field using pilot profile measurements, were made for 40, 80 and 220 kVp beams at 8.0, 1.4 and 0.2 mA, respectively. The repeatability of ISD readings was investigated by measuring six successive 30 s irradiations in an open field using 40 kVp and 80 kVp photon beams at 1.4 mAs, with no elapsed time or alteration of the experimental setup between measurements. The linearity of the output signal with dose rate for each ISD was tested by increasing the tube current setting for 30 s irradiations in an open field from 0.2 mA to 1.4 mA in increments of 0.2 mA.

B. Signal Reproducibility

The reproducibility of the signal on a day-to-day basis was investigated by measuring the variability of the output signal of ten 60 s open-field irradiations using 40 kV (at 1.4 mA) and 220 kV (at 0.1 mA), which spanned over one week. Each data point has been normalized by dividing by the mean value for each scintillator. Setup uncertainty was estimated by obtaining the standard deviation from readings taken with a single gadox-based sensor (Gd₂O₂S:Pr) after repeatedly removing and replacing the irradiation stage (with the detector bed still firmly affixed) and disconnecting and reconnecting all of the optical couplings and connections, as would normally occur between measurement sessions. This setup uncertainty value is accounted for in the reproducibility measurements by reporting only variations of the detector signals greater than the setup uncertainty. The reproducibility measurements were made within a monitored and climate controlled small animal laboratory (T = 22.7 ± 0.9 °C, ρ = 101 325 ± 3.4 Pa, RH = 41.5 ± 8.2%). However, the measurements were not corrected for temperature, pressure or humidity to include any output volatility in response to changing environmental factors.

C. Profiles

Therapy beam profiles for the 220 kVp beam were acquired in-air using 10 x 10 mm² and 5 x 5 mm² square fields at an SDD of 35 cm using the Gd₂O₂S:Tb and ZnS:Ag ISDs. For each detector, an estimation of the stage coordinates required to position the detector at the same point of entry in the beam penumbra was made by making pilot measurements at the field edge. Once this first point was estimated, profile measurements were made along the direction of the SARRP x-axis in steps of 0.25 mm (0.5 mm in areas of constant slope) under the assumption that each detector was initially located at the same off-axis distance. A 30 s irradiation time was used for each measurement point. The relative signal intensities for each ISD profile were then measured and compared to the same measurements made with the BCF-60 PSD, which was previously characterized using the 220 kVp therapy and 40, 50, 60, 70, and 80 kVp imaging beams on the SARRP [6].

D. CT Imaging

Cone beam microCT images were taken of the four ISD sensing tips and reconstructed to produce 3D representations of the high-density active volume. The images were taken on a vivaCT 40 (Scanco Medical, Bruttisellen, Switzerland) with a 70 kVp beam at 114 μA.

IV. RESULTS

A. Relative Scintillator Output

The relative signal output generated by each detector for each beam parameter set, reported as multiples of the PSD signal, can be found in Table 2. The output of each ISD has been normalized to account for their 47% larger active volumes. Relative to the BCF-60 output, each of the gadox-based scintillators' sensitivities increased with increasing energy, whereas the ZnS:Ag detector was least sensitive at the highest energy. Overall the Gd₂O₂S:Tb scintillator had the highest relative output at all energies, with up to 219 times the signal generated by the BCF-60 detector.

TABLE 2

COMPARISON OF THE SIGNAL INTENSITIES GENERATED BY EACH SCINTILLATING PHOSPHOR IN MULTIPLES OF THE LOWEST INTENSITY SIGNAL (BCF-60) FOR EACH BEAM ENERGY.

Phosphor	40 kVp	80 kVp	220 kVp
Gd ₂ O ₂ S:Tb	116	205	219
Gd ₂ O ₂ S:Eu	20	37	40
Gd ₂ O ₂ S:Pr	76	134	140
ZnS:Ag	27	29	11
BCF-60	1	1	1

B. Repeatability

Table 3 shows the mean absolute percentage deviation (MAPD) and standard deviation values for the signal intensity measurements of six consecutive irradiations using the 40 and 80 kVp beams. The Gd₂O₂S:Tb and Gd₂O₂S:Pr ISDs demonstrated excellent repeatability, with MAPD values <0.15% at both energies.

TABLE 3

STANDARD DEVIATION AND MEAN ABSOLUTE PERCENTAGE DEVIATIONS OF THE REPEATABILITY MEASUREMENTS OF EACH ISD.

Phosphor	40 kVp		80 kVp	
	MAPD	σ	MAPD	σ
Gd ₂ O ₂ S:Tb	0.13%	0.49%	0.11%	2.64%
Gd ₂ O ₂ S:Eu	0.65%	0.38%	0.42%	1.84%
Gd ₂ O ₂ S:Pr	0.14%	0.49%	0.08%	1.56%
ZnS:Ag	0.79%	0.70%	0.19%	0.74%

C. Linearity

The response of each detector was found to be independent of dose rate at 40 kV and 80 kV when varying the beam current from 0.2 to 1.4 mA (Figure 5 a-d). With the PMT voltage set to +700 mV, we observed that the Gd₂O₂S:Tb detector caused the electrometer to saturate at 0.2 mA for the 220 kV beam. Therefore, there was no range over which to investigate linearity with dose rate at 220 kV without altering the experimental setup.

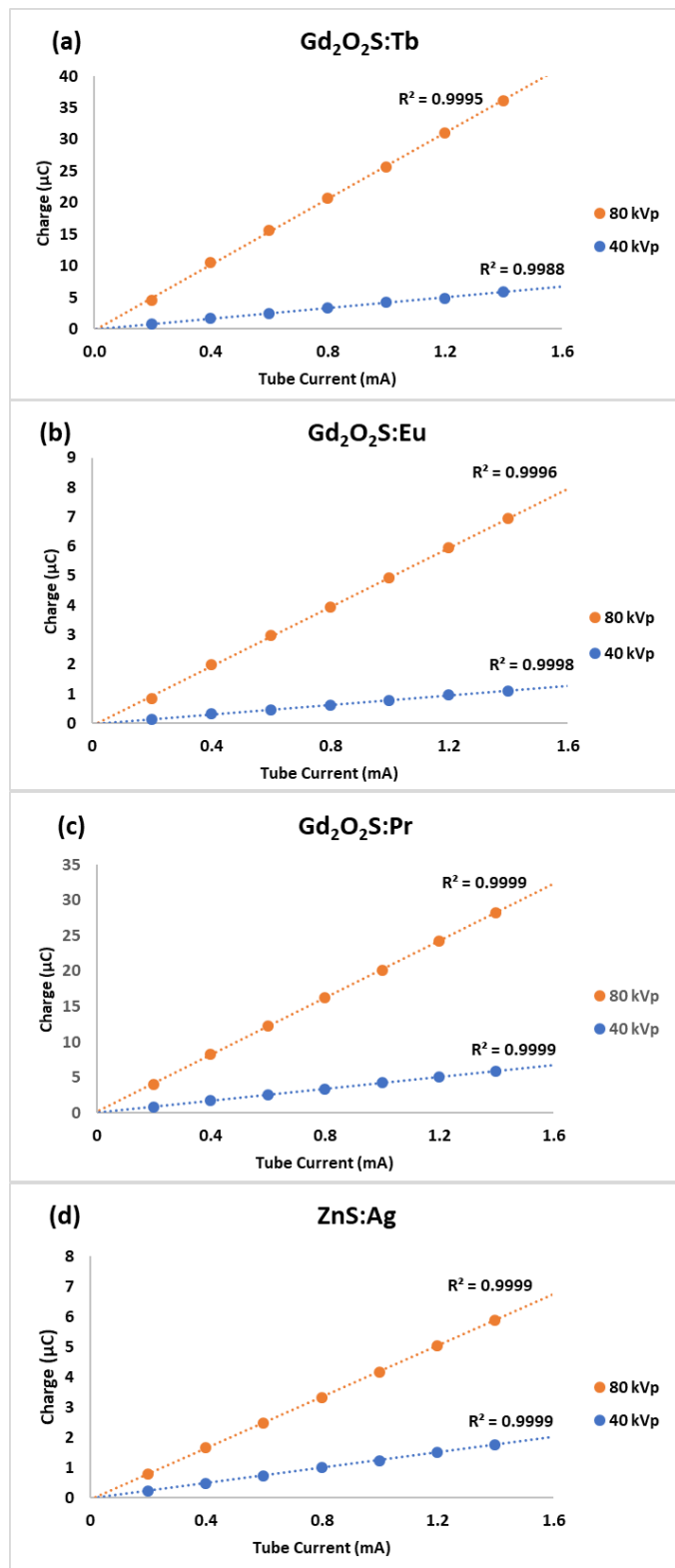


Fig. 5. (a)-(d) Linearity of the output signal of each ISD with increasing dose rate using 40 and 80 kVp beam energies.

D. Reproducibility

Figure 6 illustrates the variability of measurements made with the $\text{Gd}_2\text{O}_2\text{S:Pr}$ detector following repeated experimental setup disassembly and re-assembly. The $\text{Gd}_2\text{O}_2\text{S:Pr}$ scintillator was chosen as it had the lowest combined mean percentage difference for measurement repeatability (see Section 3.B.). The setup uncertainty measurements varied about the mean with a standard deviation of 1.8%. Figure 7 illustrates the detector signal reproducibility measurements made at 40 kVp and 220 kVp, which have been normalized using the respective mean values at each energy for each scintillator over the entire measurement period. The plots shown in Figure 7 (and their accompanying standard deviations in Table 4) have been corrected for the setup uncertainty by including only deviations greater than 1.8% (see Figure 6). All of the gadox-based ISD signals were found to be more reproducible than the BCF-60 PSD at both energies. The ZnS:Ag ISD, conversely, displayed the most fluctuation in signal intensity at both energies. It is noted that the BCF-60 results appear to stabilize around halfway through the measurement period. It is also noted that the 220 kVp measurements were less reproducible than the 40 kVp measurements.

E. Profiles

Normalized scintillator profile measurements are illustrated in Figure 8 (a) and (b). The beam profile measurements of each chosen ISD ($\text{Gd}_2\text{O}_2\text{S:Tb}$ and ZnS:Ag) were compared directly to the values of the beam profiles measured using the BCF-60 detector. For the $\text{Gd}_2\text{O}_2\text{S:Tb}$ detector, the *MAPD* of the relative intensity values were 1.1% and 1.9% for the 10×10 and 5×5 mm^2 profiles, respectively. Similarly, the *MAPD* for the ZnS:Ag and BCF-60 detector profiles were 2.5% and 6.0%, respectively. The full width at half maximum (FWHM) values for profiles measured with each ISD were also calculated and compared to the BCF-60 profile. The FWHM of the 10×10 and 5×5 mm^2 profiles measured with the $\text{Gd}_2\text{O}_2\text{S:Tb}$ detector differed by 0.3% and $<0.1\%$, respectively, relative to the BCF-60 detector profiles. The corresponding FWHM values for the ZnS:Ag detector, differed by 2.0% and 0.3%, respectively, in comparison to the BCF-60 detector profiles.

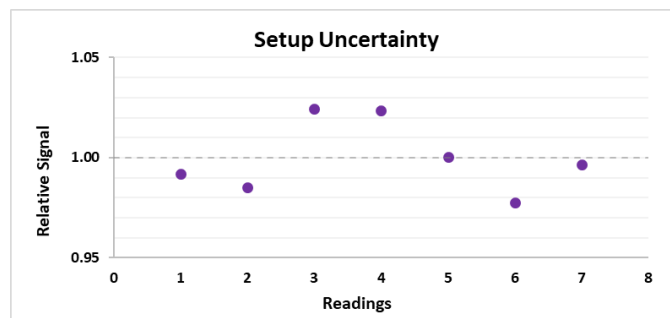


Fig. 6. Variability of the $\text{Gd}_2\text{O}_2\text{S:Pr}$ detector output signal for seven successive irradiations where the experimental setup was taken down and setup again.

F. CT Images

Figure 9 illustrates 3-D reconstructions of CT images taken of the sensing tips of each of the ISDs. The images reveal successful packing of the three gadox-based fibers. However, imaging of the ZnS:Ag phosphor reveals a filling nonuniformity in the deepest section of the cavity.

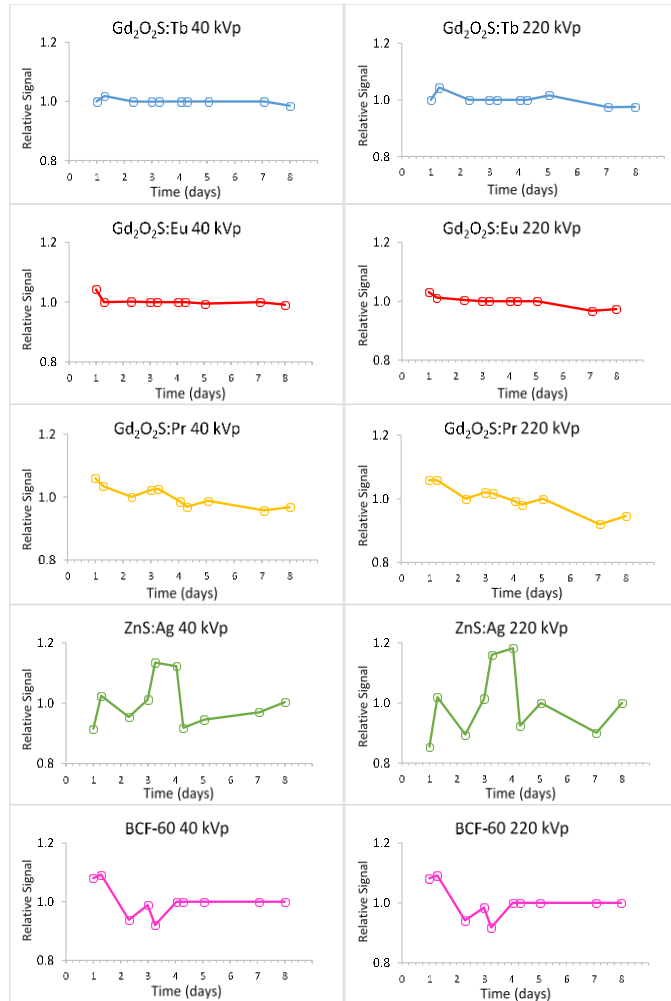


Fig. 7. Reproducibility of the signal over a period from day 1 to 8 for measurements made at 40 kVp imaging and 220 kVp therapy beam energies.. Each detectors signal is normalized to its own mean at that energy.

TABLE 4

STANDARD DEVIATION OF THE NORMALIZED REPRODUCIBILITY MEASUREMENTS SHOWN IN FIG. 7.

Phosphor	40 kVp	220 kVp
Gd ₂ O ₂ S:Tb	0.8%	1.9%
Gd ₂ O ₂ S:Eu	1.4%	1.8%
Gd ₂ O ₂ S:Pr	3.4%	4.4%
ZnS:Ag	7.7%	10.9%
BCF-60	5.3%	5.3%

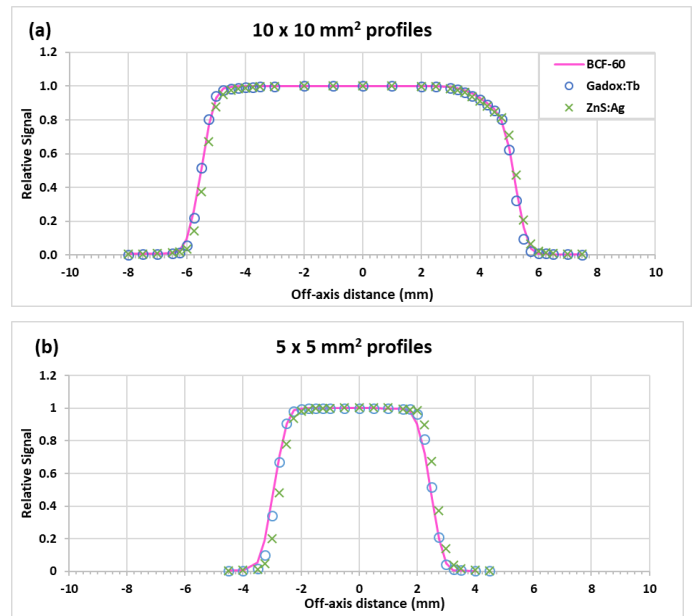


Fig. 8. (a) and (b) Lateral dose profiles obtained using the BCF-60, Gd₂O₂S:Tb and ZnS:Ag detectors.

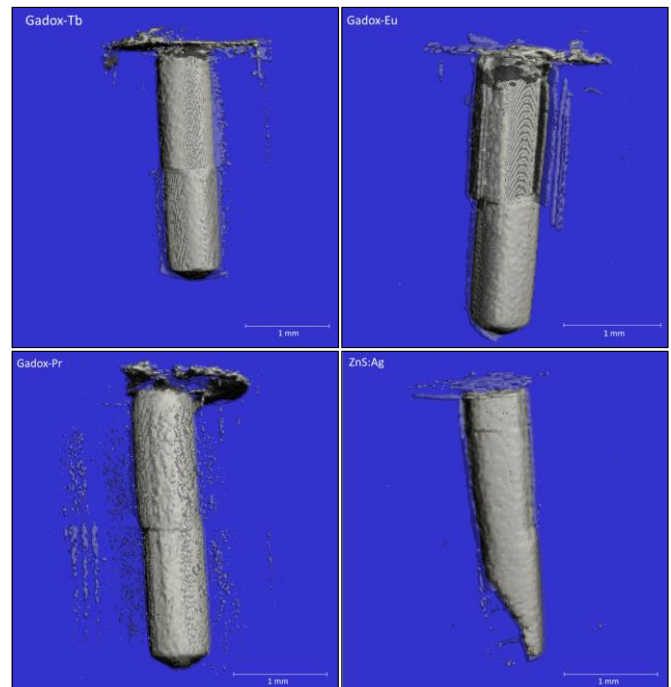


Fig. 9. 3D volume rendering based on microCT images of the four ISDs sensing tips revealing uniform packing of the dense crystal phosphor in all but the ZnS:Ag detector.

V. DISCUSSION

It is well understood that the scintillation signals carried from each of the five different materials are attenuated to varying extents due to wavelength-dependent attenuation in the PMMA OF. As the composition of all of the OFs used in this study are the same, the only inter-detector variants affecting signal attenuation are the fiber length and subsequent number of optical couplings. Each ISD has been fabricated into a 1 m length of PMMA OF, which is in turn optically coupled to a further 20 m of the same to carry signal to the PMT. As the BCF-60-based fiber was fabricated directly into a 15 m length OF, there is 6 m less PMMA optical fiber and one less optical coupling through which the PSD signal is attenuated. Despite this, the ISDs had much greater signal intensities overall. The $\text{Gd}_2\text{O}_2\text{S:Tb}$ detector had the highest signal output of all of the detectors investigated, generating up to 116 and 219 times more charge than the BCF-60 detector for the lowest energy imaging beam (40 kVp) and the therapy beam (220 kVp), respectively. One could adapt future designs to ensure all OFS had identical OF lengths.

The ZnS:Ag detector performed well in terms of measurement repeatability and linearity with dose rate but had a much lower signal output in comparison to the gadox-based scintillators. Although there is reduced perturbation of the particle fluence in the ZnS detector due to its lower density and lower (Z_{eff}) [8], it produced significantly lower signal gains (see Figure 5) due to secondary inner-filter effects [23], [24] i.e. its opacity to its own light emission [25], and less reproducible signals overall (see Figure 7). Whether in response to changes in the measurement environment – perhaps with some function of the poor packing of the active volume – or due to intrinsic fluctuations in the scintillation efficiency of the phosphor, it was also clear that the ZnS:Ag scintillator suffered the greatest variability in output over time (See Figure 7). These inner-filter effects could potentially be reduced by altering the active volume dimensions of the ZnS:Ag detector to a much shorter length, such as the $[\text{Y}_{1.9}\text{O}_3; \text{Eu}_{0.1}, \text{Li}_{0.16}]$ sensor pellet-based ISD fabricated by Belley *et al.* to perform real-time dosimetry in small animal radiation therapy [26].

It was noted that the signals measured across all detectors were less reproducible at the therapy beam energy (220 kVp) than the imaging energy (40 kVp) which was investigated (see Table 3). We attribute this to the observed difficulty of the SARRP to reduce the tube current to 0.1 mA during the ramp-up to 220 kVp before irradiation (as mentioned in Section 2.C.). This effect is further increased by the approximately linear relationship between energy fluence and tube potential squared [27].

MicroCT imaging revealed the, generally successful, packing of the crystal phosphor into the 700 μm diameter cavities of the ISDs, with just one omission. A region of dead-space is clearly visible in the deepest region of the 3 mm long cavity of the ZnS:Ag detector. This packing anomaly, along with a potentially larger error in x-axis positioning within the SARRP (as seen in Figure 8 (a) and (b)), may explain the comparatively poor performance of the ZnS:Ag fiber during beam profile measurements (2.5% and 6.0% *MADP* for the 10 x 10 and 5 x 5 mm^2 profiles, respectively).

The scintillation output of inorganic scintillators is known to have dependencies on energy and temperature. The quantum (detection) efficiency of the photodetector is wavelength dependent. Similarly, signal attenuation in the signal-carrying OF is wavelength and also length dependent. Although controlled in this study, varying environmental factors, which have not been corrected for here, will also have an effect on signal intensities measured with such a system. It was not within the scope of this study to carry out a complete characterization of the detectors. There are several variables and dependencies which would be important to control or study in detail. A full analysis of all sources of uncertainty is required in further investigations to comprehensively characterize these ISD designs for accurate dose measurements during *in vivo* dosimetry.

VI. CONCLUSION

The performance of four novel scintillator detector designs each with a 700 μm diameter, 3 mm long cavity, packed with different inorganic crystal scintillating phosphors ($\text{Gd}_2\text{O}_2\text{S:Tb}$, $\text{Gd}_2\text{O}_2\text{S:Eu}$, $\text{Gd}_2\text{O}_2\text{S:Pr}$ and ZnS:Ag) has been evaluated for the therapy and imaging beams of the SARRP. The performance of the gadox-based detectors has proven promising, with good scintillator powder packing, measurement repeatability, linearity with dose rate, and reproducibility over time. The $\text{Gd}_2\text{O}_2\text{S:Tb}$ detector, in particular, is a strong candidate for real-time dosimetry of small fields in small animal irradiators primarily because of the very large signal intensities observed. The ZnS:Ag detector, which was included to provide a lower density and, therefore, less perturbing option for the detector design, demonstrated a limited ability to measure the profiles of small radiation fields, which may be accounted for by poor packing of the phosphor cavity and an error in the positioning of the detector during irradiations. The ZnS -based detector also performed poorly in comparison to the gadox-based alternatives by way of its reduced signal intensities, which were attributed to unsuitable active volume dimensions, and lowest signal reproducibility over time. The results of this study provide a proof-of-concept for inorganic crystal phosphor-based scintillating detectors to improve the signal generation and real-time measurement capabilities suitable for dosimetric quality assurance or dose-verification purposes in preclinical trials utilizing the kilovoltage energy beams of small animal irradiators.

ACKNOWLEDGMENTS

Firstly, we would like to thank the Irish Association of Physicists in Medicine for enabling this research through the 2019 Young Investigator's Grant. We would like to thank Luc Beaulieu and François Therriault-Proulx from the Departement de Radio-Oncologie and Centre de recherche du CHU de Quebec for the use of their BCF-60 scintillating fiber. We would like to thank those at the Animal Care Facility, University of Victoria and the Medical Physics Department of BC Cancer - Victoria for their support with equipment. We would also like to thank David Connolly from the College of

Engineering and Informatics at NUI Galway for his help with the CT-imaging element of this study.

CONFLICTS OF INTEREST

We have no conflicts of interest to disclose.

REFERENCES

[1] B. F. Koontz, F. Verhaegen, and D. DE Ruyscher, "Tumour and normal tissue radiobiology in mouse models: how close are mice to mini-humans?," *British Journal of Radiology*, vol. 90, p. 20160441, 2017.

[2] J. Wong *et al.*, "A high resolution small animal radiation research platform (SARRP) with x-ray tomographic guidance capabilities," *International Journal of Radiation Oncology Biology Physics*, vol. 71, no. 5, pp. 1591–1599, 2008.

[3] R. Clarkson *et al.*, "Characterization of image quality and image-guidance performance of a preclinical microirradiator," *Medical Physics*, vol. 38, no. 2, pp. 845–856, 2011.

[4] M. Alharbi, S. Gillespie, P. Woulfe, P. McCavana, S. O. Keeffe, and M. Foley, "Dosimetric Characterization of an Inorganic Optical Fiber Sensor for External Beam Radiation Therapy," *IEEE Sensors Journal*, vol. 19, no. 6, pp. 2140–2147, 2019.

[5] C. D. Johnstone, P. Lindsay, E. E. Graves, E. Wong, J. R. Perez, and Y. Poirier, "Multi-institutional MicroCT image comparison of image-guided small animal irradiators Multi-institutional MicroCT image comparison of image-guided small animal irradiators," *Physics in Medicine and Biology*, vol. 62, pp. 5760–5776, 2017.

[6] C. D. Johnstone, F. Theriault-Proulx, L. Beaulieu, and M. Bazalova Carter, "Characterization of a plastic scintillating detector for the Small Animal Radiation Research Platform (SARRP)," *Medical Physics*, vol. 46, no. 1, pp. 394–404, 2018.

[7] J. S. Souris *et al.*, "Radioluminescence characterization of in situ x-ray nanodosimeters: Potential real-time monitors and modulators of external beam radiation therapy," *Applied Physics Letters*, vol. 105, no. 203110, pp. 1–5, 2014.

[8] A. Beddar, T. Mackie, and F. Attix, "Water-equivalent plastic scintillation detectors for high-energy beam dosimetry: I. Physical characteristics and theoretical considerations," *Physics in Medicine and Biology*, vol. 37, no. 10, pp. 1883–1900, 1992.

[9] P. Cerenkov, "Visible Radiation Produced by Electrons Moving in a Medium with Velocities Exceeding that of Light," *Physical Review*, vol. 52, no. 1, pp. 2–4, 1937.

[10] F. Theriault-Proulx, L. Beaulieu, L. Archambault, and S. Beddar, "On the nature of the light produced within PMMA optical light guides in scintillation fiber-optic dosimetry," *Physics in Medicine and Biology*, vol. 58, no. 7, pp. 2073–2084, 2014.

[11] S. Diehl, R. W. Novotny, N. Aubry, S. Faraj, and G. Ferro, "Development and Characterization of Inorganic Scintillating Fibers Made of LuAG:Ce and LYSO:Ce," *IEEE Transactions on Nuclear Science*, vol. 61, no. 2, pp. 353–361, 2014.

[12] S. O. Keeffe, D. McCarthy, P. Woulfe, M. W. D. Grattan, and A. R. Hounsell, "A review of recent advances in optical fibre sensors for in vivo dosimetry during radiotherapy," *British Journal of Radiology*, vol. 88, no. February, p. 20140702, 2015.

[13] C. W. E. van Eijk, "Inorganic scintillators in medical imaging," *Physics in Medicine and Biology*, vol. 47, pp. R85–R106, 2002.

[14] C. W. E. van Eijk, "Inorganic scintillators in medical imaging detectors," *Nuclear Instruments and Methods in Physics Research*, vol. 509, pp. 17–25, 2003.

[15] L. Archambault, A. S. Beddar, L. Gringas, R. Roy, and L. Beaulieu, "Measurement accuracy and Cerenkov removal for high performance, high spatial resolution scintillation dosimetry," *Medical Physics*, vol. 33, no. 1, pp. 128–235, 2006.

[16] A.-M. Frelin, J.-M. Fontbonne, G. Ban, J. Colin, and M. Labalme, "Spectral discrimination of Cerenkov radiation in scintillating

dosimeters," *Medical Physics*, vol. 32, no. 9, pp. 3000–3006, 2005.

[17] C. Le Deroff, A.-M. Frelin-Labalme, and X. Ledoux, "Characterization of a scintillating fibre detector for small animal imaging and irradiation dosimetry," *British Journal of Radiology*, vol. 90, p. 20160454, 2017.

[18] M. Alharbi *et al.*, "Novel optical fibre sensors and their applications in radiotherapy," in *Proceedings Volume 10680. Optical Sensing and Detection V*, 2018, no. May 2018.

[19] X. Wang *et al.*, "Photo/cathodoluminescence and stability of Gd₂O₂S:Tb,Pr green phosphor hexagons calcined from layered hydroxide sulfate," *Journal of the American Ceramic Society*, vol. 101, pp. 5477–5486, 2018.

[20] C. Michail *et al.*, "Measurement of the luminescence properties of Gd₂O₂S:Pr,Ce,F powder scintillators under X-ray radiation," *Radiation Measurements*, vol. 70, pp. 59–64, 2014.

[21] M. Nikl, "Scintillation detectors for x-rays," *Measurement Science and Technology*, vol. 17, pp. R37–R54, 2006.

[22] G. Kertzscher and S. Beddar, "Inorganic scintillation detectors based on Eu-activated phosphors for Ir-192 brachytherapy," *Physics in Medicine & Biology*, vol. 62, no. 12, pp. 5046–5075, 2017.

[23] M. Kubista, R. Sjoback, S. Eriksson, and B. Albinsson, "Experimental Correction for the Inner-filter Effect in Fluorescence Spectra," *Analyst*, vol. 119, pp. 417–419, 1994.

[24] A. V Fonin, A. I. Sulatskaya, I. M. Kuznetsova, and K. K. Turoverov, "Fluorescence of Dyes in Solutions with High Absorbance. Inner Filter Effect Correction," *PLoS ONE*, vol. 9, no. 7, 2014.

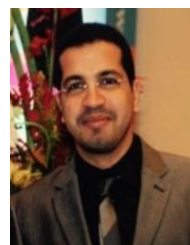
[25] G. Knoll, *Radiation Detection and Measurement*. 2010.

[26] M. D. Belley *et al.*, "Fiber-optic detector for real time dosimetry of a micro-planar x-ray beam," *Medical Physics*, vol. 42, no. 4, pp. 1966–1972, 2015.

[27] P. Allisy-Roberts and J. Williams, *Farr's Physics for Medical Imaging*. 2008.



Kevin Byrne received a B.Sc. degree in Physics with Biomedical Sciences from Dublin City University in 2018 and an M.Sc. degree in Medical Physics from the National University of Ireland, Galway in 2019. He was awarded the 2019 Young Investigator Grant by the Irish Association of Physicists in Medicine for his M.Sc. research project. His project was in collaboration with the Department of Physics and Astronomy at the University of Victoria, the Optical Fiber Sensors Research Centre at the University of Limerick and the Galway Clinic. Following his M.Sc., Kevin then received the 2019 Walton scholarship award to continue his research which concentrates on the development and characterization of novel scintillating detectors utilizing inorganic scintillating phosphors for small animal irradiation dosimetry. He is a member of the Irish Association of Physicists in Medicine.



Majed Alharbi received the B.S. in physics from Umm Al-Qura University, Saudi Arabia, in 2004, and M.S in Medical Physics from the National University of Ireland Galway in 2014. He is currently pursuing the PhD degree in Medical Physics from the National University of Ireland Galway. His PhD is collaborative

research project includes the School of Physics, the Institute of Cancer Research in London, the Optical Fiber Sensors Research Centre at the University of Limerick and the Dept. of Radiotherapy Physics in the Galway Clinic. The aim of which is to characterize novel optical fiber sensors, benchmark their response against Monte Carlo models and commercially available detectors. The novel sensor can then be used in a wide variety of applications such as to investigate the dosimetric effect of using ultrasound imaging for image guidance for radiotherapy.

Nolan Esplen received a B.Sc. degree in Physics and Astronomy in 2014 from the University of Victoria, where he is currently pursuing a Ph.D. degree in Medical Physics. As a member of the X-ray Cancer Imaging and Therapy Experimental (XCITE) lab, his doctoral research concerns the development of technologies to support the delivery of novel radiotherapy techniques, including microbeam and ultra-high dose-rate (FLASH) radiotherapy, using both conventional x-ray sources and the unique infrastructure of the Advanced Rare Isotope Laboratory (ARIEL) electron accelerator at TRIUMF.



Peter Woulfe received an M.Sc. degree in medical physics in 2003 from the National University of Galway, where his thesis focused on the development of a novel chest phantom for digital radiography. On completion of the M.Sc. degree he worked at the National Centre Laser Applications (NCLA) which led him to his current role as a Radiotherapy Medical Physicist in the Galway Clinic, progressing from a trainee physicist in 2004 to Medical Physicist Expert in 2009 and currently Principal Medical Physicist, leading a team of five Physicists in the clinic. Since 2012 he has undertaken a part-time Ph.D. degree with the Optical Fiber Sensor Research Centre (OFSRC), University of Limerick, developing radiation dosimeters for monitoring patient doses received during radiotherapy for cancer treatment.



Dr Sinead O'Keeffe is a Royal Society – Science Foundation Ireland University Research Fellow at the University of Limerick. She graduated with BE (hons) in Electronic Engineering from the University of Limerick in 2003 and received her PhD in 2006 from the same institute, for the development of polymer optical fiber sensors for the sterilization industry. On completion of her PhD, she worked as a Marie Curie Research Fellow in the General Engineering Research Institute at Liverpool John Moores University, developing optical fiber sensors for monitoring UV and Ozone. She returned to the Optical Fiber Sensors Research Centre at the University of Limerick in 2008 and was awarded an FP7 Marie Curie Research Fellowship developing radiation dosimeters for monitoring patient doses received during radiotherapy for cancer treatment. She is currently a Royal Society – Science Foundation Ireland University Research Fellow leading a team that focuses on the development of optical fiber based sensor systems for the diagnosis, assessment and treatment of cancer tumors. She was Chair of the highly successful and recently completed COST Action TD1001 aimed at developing fiber optic sensor systems for reliable use in safety and security relevant applications in society. She is

Member-at-Large of the IEEE Sensors Council for 2017-2020 and Vice-Chair of the IEEE Sensors Council UKRI Chapter (2016-2018).



Dr Magdalena Bazalova-Carter is an Assistant Professor and Canada Research Chair in Medical Physics (Tier 2) at the University of Victoria. She received her Ph.D. degree in Medical Physics from McGill University in 2009. She then became a postdoctoral fellow and later an Instructor in the Department of Radiation Oncology at Stanford University. She moved to the University of Victoria in 2015 where she leads the X-ray Cancer Imaging and Therapy Experimental (XCITE) lab. She studies novel x-ray imaging techniques, such as x-ray fluorescence CT and photon-counting CT, and radiotherapy modalities, such as small animal image-guided radiotherapy and microbeam and FLASH radiotherapy.



Dr Mark Foley received the B.S. and Ph.D. degrees in Physics from the National University of Ireland Galway, in 2000 and 2004 respectively. In 2004, he was offered a 3-year Postdoctoral research position on the SFI funded Webcom-G project. Since 2007, he has been a full-time permanent academic with the School of Physics, National University of Ireland Galway. He established the Medical Physics Research Cluster in 2006 and a B.S. in Physics with Medical Physics in 2007. His research interests include applications of Monte Carlo codes in Radiotherapy and novel Medical Imaging systems with collaborators nationally and internationally. He is the Academic Director of the CAMPEP accredited MSc in Medical Physics, National University of Ireland Galway.